

Nonaqueous vanadium disproportionation flow batteries with porous separators cycle stably and tolerate high current density

James Saraidaridis, Charles W. Monroe

Department of Engineering Science, University of Oxford, Oxford, OX1 3PJ

Keywords: redox flow battery; nonaqueous; vanadium acetylacetonate;
disproportionation; flow cell

Abstract

Vanadium acetylacetonate, or $V(\text{acac})_3$, provides a model chemistry for investigating the performance of nonaqueous disproportionation flow batteries. A flow reactor is developed that allows studies of efficiency, energy capacity, and power capability with respect to electrolyte flow rate and current density. Reactors incorporating a porous separator allowed $V(\text{acac})_3$ to be cycled without appreciable capacity fade at current densities up to 100 mAcm^{-2} . Experiments at the lowest flow rate, 12.5 mLmin^{-1} , revealed limitations imposed by residence time within the reactor, which manifested as high charging overpotentials. These overpotentials vanish above 25 mLmin^{-1} . A higher flow rate of 50 mLmin^{-1} yields performance similar to a cell at 25 mLmin^{-1} , but could improve performance at current densities above 100 mAcm^{-2} . Extrapolation of power density's dependence on current suggests a maximum power of 0.22 Wcm^{-2} for cells run at 206 mAcm^{-2} . Energy efficiency passes through a maximum of 71% at 40 mAcm^{-2} and the corresponding energy density suggests that the chemistry can, in principle, deliver above 13 WhL^{-1} in acetonitrile solutions and above 24 WhL^{-1} in mixed-solvent solutions

with higher $V(acac)_3$ solubility. A $V(acac)_3$ cell run at 40 mAcm^{-2} is shown to exhibit stable capacity and performance for more than 150 cycles.

1. Introduction

Policymakers are increasingly suggesting – and even mandating – that energy storage be incorporated into electricity grids.¹ Pumped-water plants comprise most existing grid-storage capacity,¹ but such plants are limited to sites where two large reservoirs can be maintained at disparate heights. Electrochemical energy storage has garnered both attention and installations as the search for more versatile energy-storage resources widens.²

The redox flow battery (RFB) is an electrochemical energy storage system based on redox-active electrolytic solutions, which are stored in separate tanks that are piped through a reactor where charge exchange occurs. This configuration decouples energy content (tank volume) from power rating (reactor area) and allows project customization unavailable to other popular options like Li-ion or lead-acid batteries. RFB architecture also permits the use of many different chemistries, from the state-of-the-art aqueous all-vanadium RFB³ to promising aqueous chemistries reliant on organic redox-active species.⁴ While all-vanadium RFBs and Li-ion batteries are both competitive for grid-scale electrochemical storage, cost remains a concern; some studies go so far as to suggest that curtailment of renewable electricity would be economically preferable to any battery installation.⁵

In an attempt to explore RFB cost effectiveness, this report discusses nonaqueous RFBs based on vanadium acetylacetonate [$V(acac)_3$] electrochemistry.⁶ $V(acac)_3$ is among the first active species that was shown to be able to underpin a *disproportionation*

RFB configuration: both electrolytes have the same composition in the fully discharged state; as the battery charges, the discharged species splits into reduced and oxidized forms. In the case of the $\text{V}(\text{acac})_3$ disproportionation RFB, the discharged electrolyte contains a given molarity of $[\text{V}(\text{acac})_3]^0$, which charges to $[\text{V}(\text{acac})_3]^-$ and $[\text{V}(\text{acac})_3]^+$ in the negative and positive electrolytes, respectively. Disproportionation RFBs have been referred to as ‘symmetric’ because of their compositional symmetry in the discharged state, but this symmetry breaks upon charging. Disproportionation RFBs could be constructed with alternative electrode, or catalyzed electrode, compositions that break the compositional symmetry of the discharged state, however. Furthermore, the term ‘symmetric’ has been adopted for a variety of half-cell RFB experiments that probe reaction kinetics by feeding both anode and cathode from a single reservoir. For clarity, this paper will refer to systems based on electrochemistry similar to $\text{V}(\text{acac})_3$ as disproportionation RFBs, but the results can be compared to some RFB chemistries that have previously been described as ‘symmetric’.

In any case, the class of disproportionation RFBs may lower both operational and installation costs from traditional RFB systems, even those based on single metals. Disproportionation RFBs reduce the need for periodic active-liquid generation, and may obviate the need for highly selective separator membranes.⁷

Nonaqueous RFB chemistries have been pursued because they can operate at higher voltage, thereby lowering the amount of active species needed to achieve a given energy density.⁷ Most tests of nonaqueous chemistries in the literature have involved batch electrolysis of stagnant liquids; if nonaqueous RFB technology is to mature, tests should better reflect practical circumstances. As more nonaqueous chemistries are

discovered, it is critical that performance be evaluated in flow reactors, to allow clear comparison with the dominant aqueous alternatives. Whereas laboratory-scale aqueous RFB reactors are readily available from various battery and fuel-cell suppliers, these systems often employ materials that are chemically incompatible with typical nonaqueous RFB materials.

This paper presents a custom flow cell designed specifically for chemical compatibility with nonaqueous solutions, and for resistance to corrosive high-voltage battery solutions. The reported design builds off of reports of similar cells that have been reported,^{8,9,10} and aims for straightforward reproducibility by other researchers by incorporating commercially available materials and simply machined parts.

The nonaqueous demonstration flow cell is employed to investigate control factors that affect the practical performance of the well-studied nonaqueous $\text{V}(\text{acac})_3$ disproportionation RFB chemistry.⁶ A previous flow-cell study by Escalante-García *et al.* focused on this chemistry and reported significant capacity loss within 20 cycles, using both ion-exchange membranes and porous separators in the reactor.⁹ The report identified the degradation of $\text{V}(\text{acac})_3$ to $\text{VO}(\text{acac})_2$ as the cause of capacity loss in cells run within a glovebox containing 250 ppm of water vapor – a documented source of degradation.⁷ Furthermore, when reproduced with non-proprietary materials, the system used in the study was found to have several issues, such as graphite flow plates that ‘sweat’ battery solution, that have since been resolved.¹⁰ Taking the strict control of ambient conditions and material compatibility into account in our reactor design, we find complete capacity retention over the same 20-cycle procedure without the need for stringent voltage cutoffs during charge/discharge. This is consistent with spectroelectrochemical studies that

showed no signs of electrolysis-induced $\text{V}(\text{acac})_3$ degradation for either the positive or the negative redox couple.¹¹

The power capabilities of nonaqueous vanadium disproportionation RFBs with low-cost porous Celgard 4560 separators are also explored at various electrolyte flow rates. Nonaqueous RFB research has received criticism that the chemistry cannot support practical current densities.¹² The present study addresses this debate by showing that even with a relatively low 0.1 M active-species concentration, current densities up to 100 mAcm^{-2} can readily be supported by $\text{V}(\text{acac})_3$ in a flow-through cell without any special optimization for power performance. Analysis of charge/discharge performance also reveals the voltage signatures of transport limitations within the cell, which can be induced by driving high currents at low liquid flow rates.

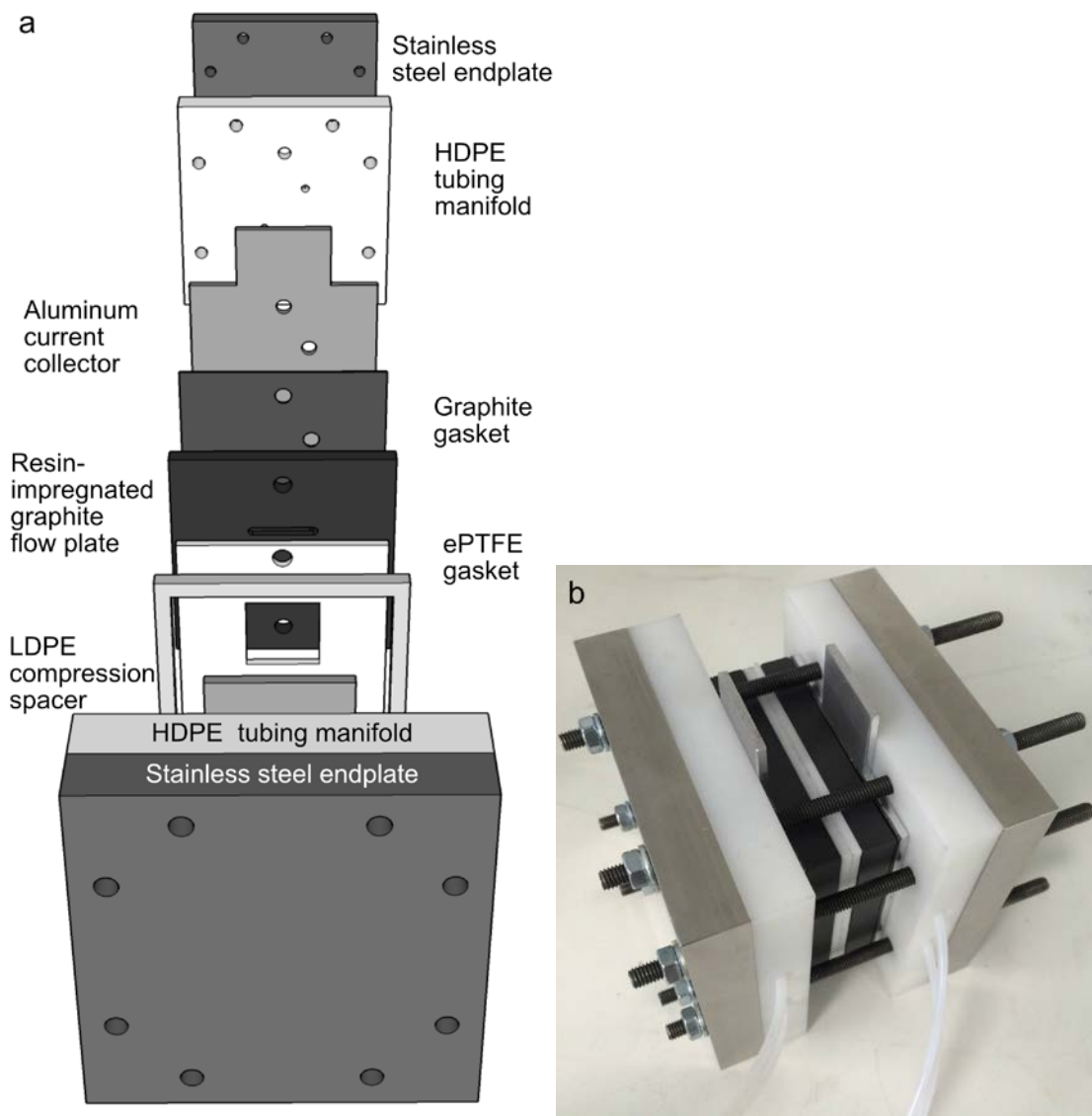


Figure 1. (a) Cell schematic showing individual components of one half of the reactor (the other half is a mirror image); (b) a photograph of the constructed cell

2. Experimental

Battery solutions were prepared using anhydrous acetonitrile (ACN) as received, (99.8%, Sigma, UK) or dried over molecular sieves (4Å, Fisher Scientific, UK) when indicated below. Tetraethylammonium tetrafluoroborate (TEABF₄) was used as received (Sigma, 99%, UK). V(acac)₃ samples from two suppliers (97%, Sigma, UK or 98%, Strem, UK) were compared and used as indicated. Water content was measured with a C30 Karl Fischer Coulometer (Mettler-Toledo, UK). Solution conductivity was measured using a Thermo Scientific Orion Star A215 pH/conductivity benchtop multiparameter meter. Solution density and viscosity were measured at 22.0 °C using an Anton Paar DMA 4100M densitometer and Lovis 2000 M/ME rolling-ball viscometer.

The cell design employed in this study is illustrated in Figure 1. Photographs of the reactor construction process and additional schematics can be found in the supplementary information that accompanies this article, Figure S1. Multipurpose 304 stainless steel (McMaster-Carr, USA) was machined into 110 mm x 110 mm x 17 mm endplates with 6.35 mm diameter holes bored to allow cell compression *via* 6 mm 316 stainless steel threaded rods. Rigid HDPE polyethylene (McMaster-Carr, USA) was machined into 110 mm x 110 mm x 17 mm tubing manifolds with corresponding bolt-holes, and two 6.35 mm diameter centering-pin guides. Two 4 mm diameter, 8.5 mm deep tubing-outlet bores were connected perpendicularly with two 6.35 mm diameter tubing-inlet bores to provide access through the tubing manifold to the reactor cell *via* PTFE tubing. These manifolds serve three purposes: insulate the cell from an endplates-to-bolt short-circuit; provide a path for 1/8" OD, 1/16" ID tubing (PTFE from Fisher Scientific, UK or fluorinated ethylene propylene (FEP) coated Teflon from McMaster-

Carr, USA); and provide a rigid face for a compression seal *via* o-rings and the rigid face of the graphite flow-plate. Corrosion-resistant 6101 aluminum (McMaster-Carr, USA) was machined into 80 mm x 80 mm x 3.2 mm current collectors with two 6.35 mm guides for centering-pins, two 6.35 mm holes for a tubing-path/compression-fitting, and a 40 mm x 25 mm tab for electrical connection. A 1/32" high-temperature graphite gasket (McMaster-Carr, USA) cut to the size of the current collector and punched with 6.35 mm holes for the centering-pins and tubing sits between the aluminum current collector and graphite flow-plates. Impervious bipolar graphite (Graphitestore.com, USA) was machined into 80 mm x 80 mm x 6.35 mm flow-plates with two 6.35 mm guides for centering-pins and two 25 mm x 3.175 mm x 3 mm flow-collector- recesses framing the square 25 mm x 25 mm cell reactor area. A single 3.175 mm tubing-inlet bore was drilled into each recess such that they were positioned diagonally at opposing corners of the square reactor area.

For assembly, the 1/8" OD PTFE tubing was wound through the HDPE flow manifold, current collector, gasket, and ultimately, the flow plate. Three o-rings were placed around the tubing between the manifold and flow-plate: two Viton on the manifold side, and one FEP-coated Viton on the flow-plate side (McMaster-Carr, USA). This construction formed a solvent-tight seal under compression. Expanded PTFE gaskets (ePTFE, 3.125 mm thick uncompressed, McMaster-Carr, USA and Polyflon, UK) were cut to 70 mm x 70 mm, with two 6.35 mm guides punched for centering-pins and a 25 mm x 25 mm reactor area cut to fit carbon felt electrodes. Finally, a single 80 mm x 80 mm x 3 mm LDPE spacer (McMaster-Carr, USA) enveloped the outer edges of the two ePTFE gaskets and provided a compression guide. Upon construction, the eight bolts

were tightened with a torque wrench to 50 in-lb in a 4-2-4-3 pattern until all bolts maintained the desired torque. This torque was found to compress the two ePTFE gaskets sufficiently that they became flush with the single 3 mm LDPE spacer. All construction occurred within an Inert PureLab argon-filled glovebox with <1.0 ppm O_2 and H_2O .

2.1 Reactor Components

Cell electrodes consisted of 3.18 mm thick carbon felt (Alfa-Aesar, UK) cut into 25 mm x 25 mm squares. Before use, the carbon-felt electrodes were heated to 250 °C for 48 hours under vacuum to remove residual water. During construction, the felt was placed into the void of the ePTFE gasket and subsequently compressed to 1.5 mm thickness – a compression ratio of 53%. The Celgard 4560 separator, which consisted of a 25 μ m polypropylene membrane laminated onto a 110 μ m nonwoven polypropylene support fabric, was cut into 50 mm x 50 mm squares and heated at 75 °C for two hours in ambient air before being brought into the glovebox, wherein it was allowed to cool. Before use in the cell, the separator was soaked in neat ACN for two hours. Upon construction, the separator was sandwiched between the two expanded PTFE gaskets. Fresh separator membranes were used each time the flow cell was assembled.

2.2 Testing procedure

Electrolyte flows through the cell were oriented co-currently and flow rates were calibrated with battery solution at open circuit before initiating each charge/discharge test. Both reactor chambers were loaded with solution before diverting the reactor outlet line to a graduated cylinder for flow calibration. Flow rate calibrations targeted 50 mL

total of pumped fluid into the graduated cylinder, leading to 4-minute, 2-minute, and 1-minute calibration test periods for the 12.5, 25 and 50 mLmin⁻¹ flow rates, respectively. If flow rates did not achieve the necessary pumped volume, the pump speed of the Masterflex L/S PTFE Tubing Pump (Model 77390, Cole-Parmer, UK) with 6-mm PTFE pump-head tubing (Cole-Parmer, UK) was adjusted and the calibration test was rerun. Notably, these are average flow rates: the peristaltic pumps deliver a flow rate that fluctuates around this mean value. Especially for an RFB using a porous separator, these fluctuations in flow rate can induce small pressure differences across the separator that drive net electrolyte transfer from one electrolyte reservoir to the other and lead to subsequent coulombic inefficiency. This imbalancing phenomenon and its impact on performance will be a topic of further study. Once both pumps were calibrated, the battery solution was vacated from the cell and the 100 mL of electrolyte was split between the two battery reservoirs. Subsequently, the pumps were restarted and the cell was prepared for electrochemical testing.

2.3 Degradation testing

Electrochemical impedance spectroscopy (EIS) was used to evaluate the changes in electrolyte properties during testing. Impedance spectra were collected for both a stagnant cell and a cell with electrolyte flow, both before charge/discharge experiments and after. A 10 mV RMS signal amplitude was used, and impedance was gathered over frequencies ranging from 50 kHz to 0.1 Hz with eight points per decade. EIS was performed using an Autolab PGSTAT 302N potentiostat with the FRA32 module (Metrohm, UK). Cyclic voltammograms of the battery electrolyte were collected for both

the positive electrolyte and negative electrolyte after completion of charge/discharge cycling and EIS measurements. The voltage was swept between -2.2 V and 1.0 V vs. Ag/Ag^+ at 400 mVs^{-1} . A 1 mm diameter glassy carbon electrode (Basi Inc.) served as the working electrode and a 30 cm long, 0.3 mm diameter coiled platinum wire dipped in the same solution, but in another chamber separated from the working electrode by a glass frit, served as counter electrode. The Ag/Ag^+ reference electrode consisted of a silver wire submerged in an ACN solution of 0.01 M AgNO_3 and 0.05 M TEAClO_4 . In addition to atmospheric control, the glovebox provided temperature control for the experiments (ambient temperatures were $21.5 \pm 2^\circ\text{C}$).

2.4 Charge/discharge procedure

Charge/discharge experiments with the $0.1 \text{ M V}(\text{acac})_3 / 0.5 \text{ M TEABF}_4 / \text{ACN}$ battery solution were controlled *via* either an Autolab PGSTAT 302N potentiostat or Maccor 4000 series battery tester (Maccor, USA). The procedure involved an initial charge to 75% of the theoretical maximum state of charge (SOC), with all subsequent discharges and charges across 50% theoretical SOC as computed via coulomb counting, or until voltage cutoffs were reached, whichever came first. Theoretical SOC was calculated using the initial active-species concentration and assuming a single-electron disproportionation $\text{V}(\text{acac})_3$ reaction. Voltage cutoffs of 3.7 V on charging steps or 1.0 V on discharging steps were applied. Either the delivery or removal of 50% theoretical SOC or passing the voltage cutoffs triggered a switch to the next cycling step. Experiments were performed at 10 , 20 , 40 and 100 mAcm^{-2} current densities on cells employing 12.5 , 25 and 50 mLmin^{-1} flow rates. The area-specific molar flow rates and stoichiometric

ratios for this experimental matrix are included in Table 1. On some occasions, reservoirs were observed to accumulate volume imbalances; these imbalances were ascribed to imperfect flow calibration and deterioration in pump performance over the course of a cycling experiment. Simply transferring electrolyte directly from the rich reservoir to the poor reservoir was found to rectify the imbalance without any observed effects after the cycle in which the transfer occurred, as would be expected for a disproportionation RFB chemistry.

Table 1. Disproportionation RFB charge/discharge experimental parameters assuming reactant streams at 0% (or 100%) SOC. All area-specific quantities, including current densities, are normalized by the membrane area exposed to the reactor chambers, 6.25 cm². The free volume through which liquid flows is 0.90 mL in both electrode chambers.

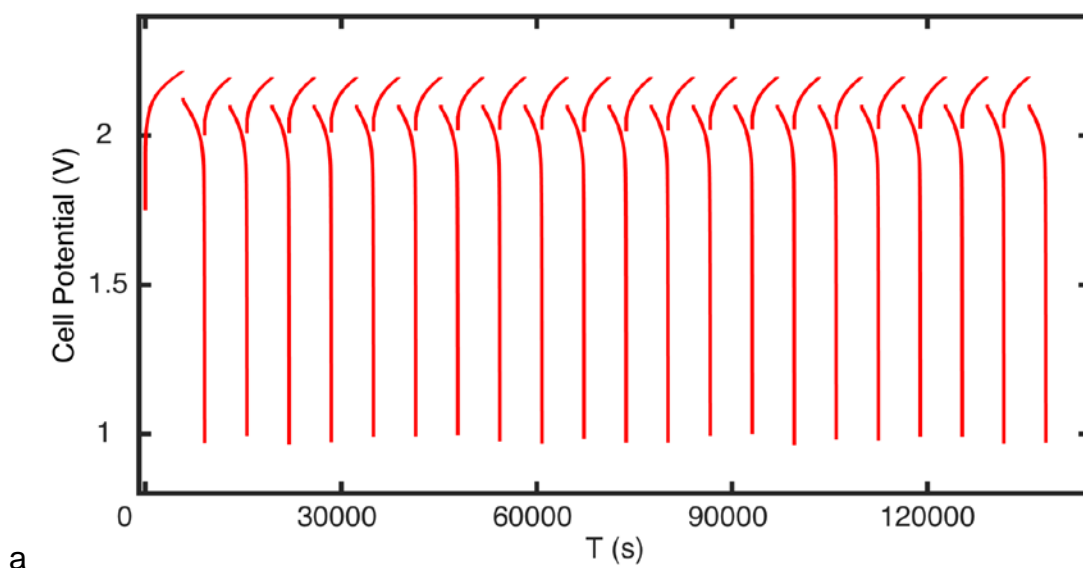
	12.5 mLmin ⁻¹		25 mLmin ⁻¹		50 mLmin ⁻¹	
	Area-specific molar flow (molcm ⁻² s ⁻¹)	Stoichio-metric ratio	Area-specific molar flow (molcm ⁻² s ⁻¹)	Stoichio-metric ratio	Area-specific molar flow (molcm ⁻² s ⁻¹)	Stoichio-metric ratio
10 mAcm ⁻²	3.33 x 10 ⁻⁶	32.2	6.67 x 10 ⁻⁶	64.3	1.33 x 10 ⁻⁵	128.6
20 mAcm ⁻²		16.1		32.2		64.3
40 mAcm ⁻²		8.0		16.1		32.2
100 mAcm ⁻²		3.2		6.4		12.9

3. Results and Discussion

3.1 Battery-Solution Characterization

Since previous reports revealed that the presence of water leads to a degradation pathway for V(acac)₃,⁷ Karl Fischer titration was used to quantify the water content of solution components. As-received anhydrous ACN samples had water contents of 29.2 ± 2.0 ppm. Solutions of TEABF₄ in ACN at various concentrations had similar water contents of 28.3 ± 4.7 ppm, indicating the lack of appreciable moisture in the salt precursor. Storage over 4 Å molecular sieves for 24 hours reduced water content in ACN samples by an order of magnitude, to 2.8 ± 0.7 ppm. The conductivity of 0.5 M TEABF₄ in ACN was measured and found to be 43 mScm⁻¹.

The voltammogram of Strem-provided $\text{V}(\text{acac})_3$ delivers the expected redox couples at -1.79 V and $0.41\text{ V vs. Ag/Ag}^+$, as shown in Figure S2 of the supplementary information. Voltammetry with solutions of $\text{V}(\text{acac})_3$ received from Sigma, which was used in the Escalante-Garcia study,⁹ shows clear evidence of impurity. The voltammogram of Sigma-provided $\text{V}(\text{acac})_3$, also shown in Figure S2, produces noticeably smaller redox peaks and a redox couple at $0.71\text{ V vs. Ag/Ag}^+$ that indicates the presence of $\text{VO}(\text{acac})_2$.⁷ The Strem samples were delivered in wax-sealed, argon-filled, amber screw-top bottles packaged in airtight tins filled with hygroscopic vermiculite. The Sigma samples were merely sealed in amber screw-top bottles under ambient atmosphere and packaged in bubble wrap. Ambient moisture exposure has been shown to be responsible for degradation of $\text{V}(\text{acac})_3$ to $\text{VO}(\text{acac})_2$,⁷ and the different delivery conditions could explain the discrepancy in precursor quality. Since the prices were comparable between the suppliers, Strem-supplied $\text{V}(\text{acac})_3$ was used for all subsequent experiments.



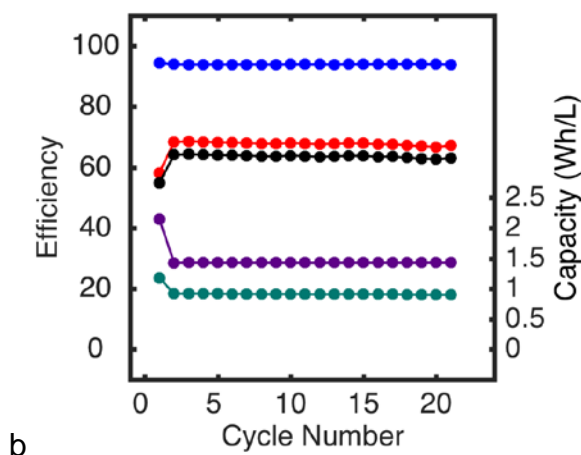


Figure 2. Galvanostatic charge/discharge cycling a) curves at 10 mAcm^{-2} and 25 mLmin^{-1} and b) performance: voltage efficiency (blue), coulombic efficiency (red), energy efficiency (black), energy capacity on charge (purple), energy capacity on discharge (green).

3.2 Capacity retention

Charge/discharge experiments for $\text{V}(\text{acac})_3$ under the conditions investigated by Escalante-García *et al.*⁹ were repeated, with more stringent atmospheric control and using battery solutions dried over molecular sieves, which were also tested to be free of observable $\text{VO}(\text{acac})_2$ impurity. The procedure also eliminated the strict 2.27 V charging cutoff used in the prior study.

The cells studied here were run using 0.1 M $\text{V}(\text{acac})_3$ with 0.5 M TEABF_4 in ACN, with a 10 mAcm^{-2} current density and 25 mLmin^{-1} electrolyte flow rates. Immediately apparent from the first cycle in Figure 2 is a ‘burn-in’ inefficiency across the first cycle. The rest of the cycles depicted in Figure 2 show that batteries using solutions free of vanadyl species and without significant water impurity do not succumb to capacity fade; the cell cycles reproducibly after burn-in. The system averages 68% coulombic efficiency, 94% voltage efficiency, and 64% energy efficiency. These percentages are consistent with results from the previous study, agnostic to the capacity

fade observed there. The cell delivers an energy density of 0.91 WhL^{-1} and an average power density of 20.3 mWcm^{-2} . Whereas discharge capacity faded in the previous experiments by over 80% after ten cycles, the present experiments delivered a final discharge capacity within 1% of the average capacity across cycles 4-21. Additionally, the stringent voltage cutoffs described in the previous report⁹ were found to be unnecessary for stable cycling.

EIS data from before and after cycling, shown in Figure 3, reveal little change in the impedance; the low-frequency response changes somewhat, likely because of the difference in open-circuit potential between the beginning and end of cycling. The bulk area-specific resistance (ASR), as determined by the intercept of the impedance curve with the real axis, is relatively constant before and after cycling: $4.6 \text{ }\Omega\text{cm}^2$ and $4.5 \text{ }\Omega\text{cm}^2$, respectively. A second ASR value, as determined by a semicircle fit to the high frequency data, is $8.1 \text{ }\Omega\text{cm}^2$ before cycling and $7.4 \text{ }\Omega\text{cm}^2$ after. The underlying source of this second ASR is unclear since an ASR of that magnitude at the current density applied in the cycling experiments would equate to voltage efficiencies below the 94% observed. Furthermore, the control experiment lacking any redox-active solution components shown in Figure S3 exhibits similar high-frequency behavior. Thus it appears that this apparent semicircular feature results from the supporting-electrolyte-immersed porous flow-through electrode, rather than the reaction kinetics of the $\text{V}(\text{acac})_3$ compound.

Cyclic voltammograms of the electrolyte before and after charge/discharge testing, included in Figure S4 of the supplementary information, show similar redox behavior to the pristine solution (Figure S2): the reduction and oxidation peaks at -1.8 and $0.4 \text{ V vs. Ag/Ag}^+$ still dominate.⁹ Some small differences in the voltammograms are

observed after the 21 cycles. The cycled negative electrolyte delivers a smaller absolute reduction-peak height within the reduction couple. The cycled positive electrolyte shows evidence of a very dilute VO(acac)₂ couple centered at 0.7 V vs. Ag/Ag⁺, as well as a small oxidative peak at -1.0 V vs. Ag/Ag⁺, which has been observed in systems with added acetylacetone.¹³

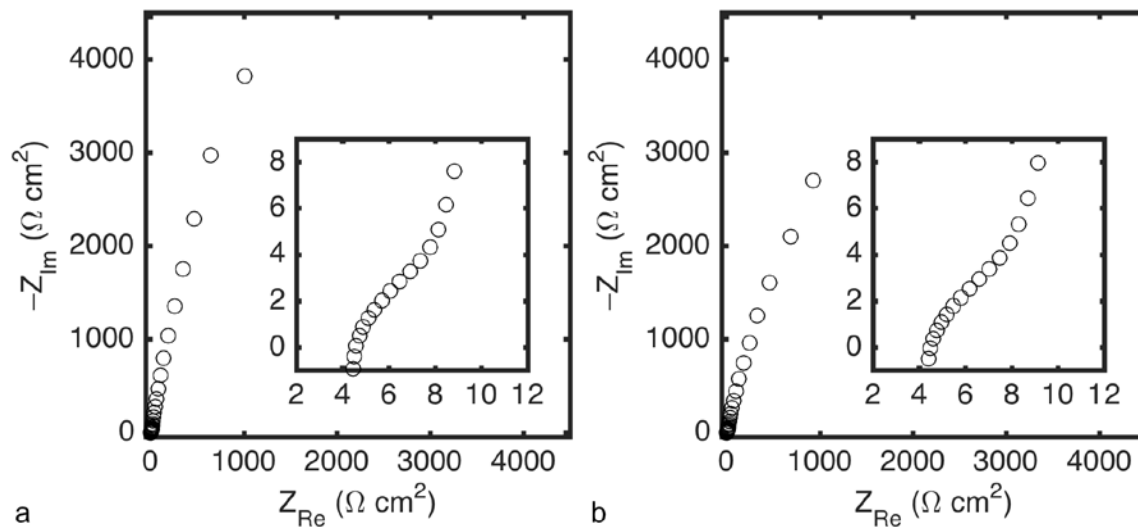


Figure 3. Nyquist plots from EIS experiments on flow cell with stagnant 0.1 M V(acac)₃, 0.5 M TEABF₄ in ACN battery solution a) before b) after charge/discharge testing. Insets show the system response at high frequencies.

3.3 Performance variation with flow rate and current density

Having demonstrated the stable cyclability of the V(acac)₃ disproportionation chemistry, the system was used to explore two more general questions. First, how does changing cell operating parameters such as flow rate affect performance metrics like energy density, power density, and efficiency of nonaqueous disproportionation RFBs? Second, are nonaqueous RFBs subject to transport limitations that will severely handicap them compared to aqueous systems, as suggested by Sun *et al.*?¹²

This experimental protocol entailed cycling cells across a procedural matrix formed by charge/discharge experiments run at 12.5, 25, and 50 mLmin⁻¹ and 10, 20, 40, and 100 mAcm⁻². A comparison of system performance metrics across a range of liquid flow rates and electric current densities is presented in Figure 4.

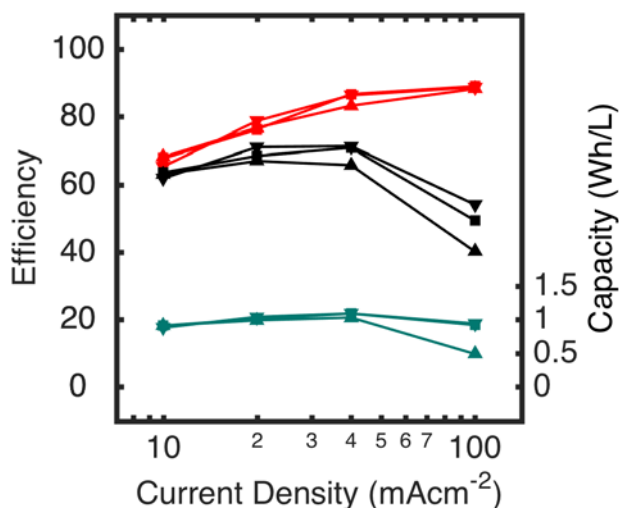


Figure 4. Flow rate dependence (upward triangle – 12.5 mLmin⁻¹, square – 25 mLmin⁻¹, downward triangle – 50 mLmin⁻¹) on coulombic efficiency (red), energy efficiency (black), and discharge energy capacity (green).

Cells run at 25 or 50 mLmin⁻¹ provided a maximum energy density at 40 mAcm⁻² of 1.09 WhL⁻¹. Figure 4 shows that cells operated at the energy maximum exhibited 87% (86%) coulombic efficiency, 82% (83%) voltage efficiency, and 71% (71%) energy efficiency at 25 mLmin⁻¹ (50 mLmin⁻¹).

If these performance characteristics are extrapolated to cells run across 100% SOC at the solubility limit of 0.6 M,⁷ unmodified V(acac)₃ in neat ACN would offer a maximum energy density of 13 WhL⁻¹. Unmodified V(acac)₃ in mixed nonaqueous solvents has realized even higher solubility limits of 1.1 M¹⁴, which would deliver a maximum energy density of 24 WhL⁻¹. V(acac)₃ with modified acac⁻ ligands has

achieved concentrations as high as 1.3 M in neat ACN and would provide energy density of 28 WhL⁻¹.¹⁵ This last figure exceeds the 25 WhL⁻¹ offered by conventional aqueous-vanadium RFBs with 65% as much vanadium.¹⁶

Cells run at the highest current density, 100 mAcm⁻², with 25 and 50 mLmin⁻¹ flow rates, suffer from low voltage efficiencies (56% and 61%, respectively), yet deliver comparable discharge capacities (0.92 and 0.94 WhL⁻¹, respectively); the higher current densities improve coulombic efficiencies to 89% at both flow rates. These results are not surprising given the use of porous separators: higher current densities lower the stoichiometric ratio, reducing the impact of crossover; voltage efficiency is lost because there are increased ohmic losses at higher currents.

These results also reveal diminishing energy-capacity returns with respect to flow rates above 25 mLmin⁻¹. A more optimal flow rate for the current densities examined may exist between 12.5 and 25 mLmin⁻¹. Cells run at current densities corresponding to peak power may benefit from the high flow rate, however. Lower flow rates require less pumping energy and should be targeted so long as they do not introduce additional overpotentials. Nonaqueous RFBs using ACN already promise lower pumping losses than aqueous systems due to the solutions' lower viscosities (0.535 cP for the 0.1 M V(acac)₃, 0.5 M TEABF₄, ACN solution).

Whereas this matrix of experiments reveals a combination of parameters that maximizes energy density, a power density maximum is not reached. The polarization curve in Figure 5 is still trending upwards – even for the 100 mAcm⁻² trials, which deliver 0.16 Wcm⁻² at the highest flow rate. Following a model proposed by Sun *et al.* to predict the maximum power capability of RFBs,¹² the losses for the 50 mLmin⁻¹ flow

rate can be fit by a parabola under the assumption that all losses are linearly resistive.

One can express the power as

$$P = IV_{\text{OCP}} - I^2 R, \quad (1)$$

where P is the power at current I , R is the cell resistance, and V_{OCP} is the chemistry's average open-circuit potential. The power trend observed from the flow cell is fit well by a second-order polynomial, which predicts that a maximum power of 0.22 Wcm^{-2} would be reached by cells run at 206 mAcm^{-2} . More concentrated battery solutions and cell optimization should improve the maximum power density for these systems towards parity with optimized aqueous vanadium systems, which deliver 1.3 Wcm^{-2} at nearly 2000 mAcm^{-2} .¹²

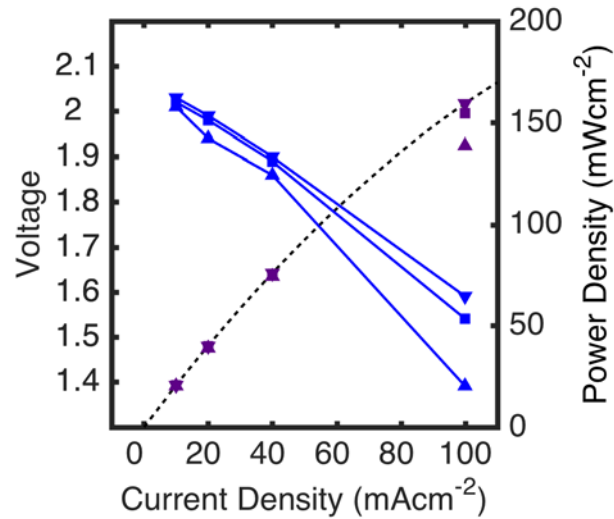


Figure 5. Flow rate dependence (upward triangle – 12.5 mLmin^{-1} , square – 25 mLmin^{-1} , downward triangle – 50 mLmin^{-1}) on average voltage (blue) and power density (purple) during discharge.

Whereas the cells run at 25 and 50 mLmin^{-1} deliver similar cell performance, the cells run at 12.5 mLmin^{-1} , especially above the lowest current density, deviate from the performance seen at higher flow rates. Specifically, cells run at 100 mAcm^{-2} present impractical decreases in discharge capacity as evidenced by the data in Figure 4, and cells

run at 20 mA cm^{-2} begin to show appreciably lower average cell discharge voltage, as shown in Figure 5. The significant decrease in both discharge capacity and voltage at low flow rates likely results from concentration overpotentials. Concentration overpotentials likely arise because reactants in the electrolytes become depleted during their residence time in the reactor and the stoichiometric ratio decreases below 1 as the SOC approaches 75% on charge, or 25% on discharge. Since residence time in the RFB cell increases at lower flow rates, reactors will deliver higher bulk conversion of active species and cause substantial concentration polarization along the flow direction in low-flow-rate systems.

3.4 Cell Longevity

In addition to experimental reports suggesting that reactors containing $\text{V}(\text{acac})_3$ active species succumb to capacity fade, Kucharyson *et al.* used density functional theory to model $\text{V}(\text{acac})_3$ in its anionic, neutral, and cationic states, and determined that the molecule would decompose with cycling.¹⁷ The researchers suggested that a negative electrolyte that supports the anionic $\text{V}(\text{acac})_3$ reaction would decompose to 80% capacity after 20 cycles, and the corresponding positive electrolyte would decompose to 80% capacity after 35 cycles. A battery chemistry with such a short cycle-life span would be impractical for applications.

To study these concerns about cell longevity beyond 20 cycles, the charge/discharge procedure was extended to 160 cycles, for which results are shown in Figure 6. Since the cycles run in this procedure range over 50% theoretical SOC, rather than the full conversion described in the molecular simulation, 40 cycles in this control

scheme would be necessary to shrink the negative electrolyte capacity to 80%. Assuming exponential decay over 160 cycles, the capacity of the negative electrolyte should decrease to 41% and the positive electrolyte to 60%. In a procedure that aims to span 50% theoretical SOC, this degradation would manifest as both capacity fade in later cycles and charge/discharge profiles that access a wider voltage on the Nernst curve. Yet Figure 6 shows stable cycling performance, reliably charging and discharging across 0–50% SOC and delivering similar voltage profiles from cycles 2 to 160.

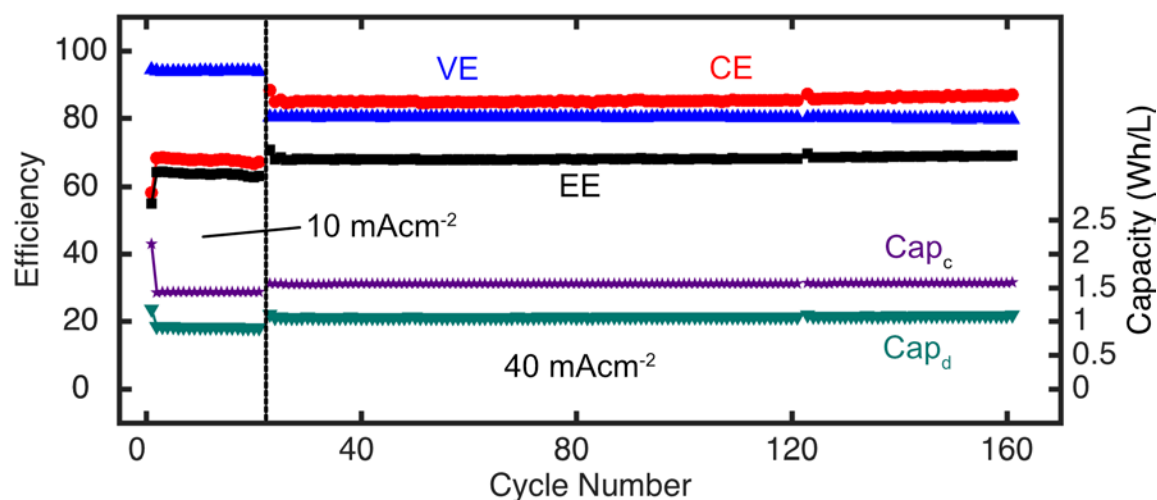


Figure 6. Performance of cell cycled for 160 cycles at 25 mLmin⁻¹: voltage efficiency (blue), coulombic efficiency (red), energy efficiency (black), energy capacity on charge (purple), energy capacity on discharge (green).

4. Conclusions

This paper addressed recently reported concerns about the cycling stability of a nonaqueous V(acac)₃ disproportionation RFB chemistry.^{9,17} In reactors using a non-selective porous separator, V(acac)₃ was demonstrated to be cyclable without appreciable capacity loss in a co-current, flow-through flow cell with strictly controlled material purity and compatibility. Admittedly, stringent purity conditions may prove impractical

in real-world applications. Flow-rate and current-density studies indicate a maximum energy efficiency and energy density at 40 mAcm^{-2} for flow rates of 25 and 50 mLmin^{-1} . These studies deliver a 0.16 Wcm^{-2} power density at 100 mAcm^{-2} with 50 mLmin^{-1} flow rates and suggest a peak power of 0.22 Wcm^{-2} would be achieved at 206 mAcm^{-2} , although this was outside the range of current densities studied. Despite not achieving the power maximum, the observed power densities were comparable to aqueous systems,¹² allaying fears of the practicality of nonaqueous RFBs for power applications. Furthermore, extended cycling studies showed stable capacity and efficiency performance over 160 cycles. These results suggest that $\text{V}(\text{acac})_3$ may have the molecular resilience to deliver the many cycles necessary for practical grid scale applications. Additionally, $\text{V}(\text{acac})_3$ can be used as an inexpensive model active species for future studies of disproportionation RFB reactors.

5. Acknowledgments

Dr. Saraidaridis was supported by Siemens Aktiengesellschaft under the studentship research contract ‘Reactors for High-Voltage Redox Flow Batteries,’ and by the ISCF Materials Research Hub for Energy Capture, Conversion and Storage (M-RHECCS), EPSRC grant no. EP/P007775/1.

6. References:

1. Jenson, J.; Pike, S., State of Charge Massachusetts Energy Storage Initiative Study. 2016.
2. UniEnergy Technologies Announces Commissioning of Largest Capacity Flow Battery in North America and Europe. <http://www.uetechologies.com>.
3. M. Skyllas-Kazacos, M. R., R. Robins, A. Fane, M Green, New All-Vanadium Redox Flow Cell. *Journal of the Electrochemical Society* **1986**, *133*, 1057-1058.
4. B. Huskinson, M. M., C. Suh, S. Er, M. Gerhardt, C. Galvin, X. Chen, A. Aspuru-Guzik, R. Gordon, M. Aziz, A metal-free organic-inorganic aqueous flow battery. *Nature* **2014**, *505*, 195-198.
5. Arbabzadeh, M.; Johnson, J. X.; De Kleine, R.; Keoleian, G. A., Vanadium redox flow batteries to reach greenhouse gas emissions targets in an off-grid configuration. *Appl. Energy* **2015**, *146*, 397-408.
6. Liu, Q. H.; Sleightholme, A. E. S.; Shinkle, A. A.; Li, Y. D.; Thompson, L. T., Non-aqueous vanadium acetylacetonate electrolyte for redox flow batteries. *Electrochemistry Communications* **2009**, *11* (12), 2312-2315.
7. Shinkle, A. A.; Sleightholme, A. E. S.; Griffith, L. D.; Thompson, L. T.; Monroe, C. W., Degradation mechanisms in the non-aqueous vanadium acetylacetonate redox flow battery. *Journal of Power Sources* **2012**, *206*, 490-496.
8. Maurya, S.; Shin, S.-H.; Sung, K.-W.; Moon, S.-H., Anion exchange membrane prepared from simultaneous polymerization and quaternization of 4-vinyl pyridine for non-aqueous vanadium redox flow battery applications. *Journal of Power Sources* **2014**, *255* (Supplement C), 325-334.
9. Escalante-García, I. L.; Wainright, J. S.; Thompson, L. T.; Savinell, R. F., Performance of a Non-Aqueous Vanadium Acetylacetonate Prototype Redox Flow Battery: Examination of Separators and Capacity Decay. *Journal of The Electrochemical Society* **2015**, *162* (3), A363-A372.
10. Milshtein, J. D.; Kaur, A. P.; Casselman, M. D.; Kowalski, J. A.; Modekrutti, S.; Zhang, P. L.; Harsha Attanayake, N.; Elliott, C. F.; Parkin, S. R.; Risko, C.; Brushett, F. R.; Odom, S. A., High current density, long duration cycling of soluble organic active species for non-aqueous redox flow batteries. *Energy & Environmental Science* **2016**, *9* (11), 3531-3543.
11. Saraidaridis, J. D.; Bartlett, B. M.; Monroe, C. W., Spectroelectrochemistry of Vanadium Acetylacetonate and Chromium Acetylacetonate for Symmetric Nonaqueous Flow Batteries. *Journal of The Electrochemical Society* **2016**, *163* (7), A1239-A1246.
12. Sun, C. N.; Mench, M. M.; Zawodzinski, T. A., High Performance Redox Flow Batteries: An Analysis of the Upper Performance Limits of Flow Batteries Using Non-aqueous Solvents. *Electrochimica Acta* **2017**, *237*, 199-206.
13. Nawi, M. A.; Riechel, T. L., Electrochemical studies of vanadium(III) and vanadium(IV) acetylacetonate complexes in dimethylsulfoxide. *Inorganic Chemistry* **1981**, *20* (7), 1974-1978.
14. T. Herr, P. F., J. Tubke, K. Pinkwart, P. Elsner, Increasing the energy density of the non-aqueous vanadium redox flow battery with the acetonitrile-1,3-dioxolane-dimethyl sulfoxide mixture. *Journal of Power Sources* **2014**, *265*, 317-324.

15. Suttill, J. A.; Kucharyson, J. F.; Escalante-Garcia, I. L.; Cabrera, P. J.; James, B. R.; Savinell, R. F.; Sanford, M. S.; Thompson, L. T., Metal acetylacetonate complexes for high energy density non-aqueous redox flow batteries. *Journal of Materials Chemistry A* **2015**, 3 (15), 7929-7938.
16. Li, L.; Kim, S.; Wang, W.; Vijayakumar, M.; Nie, Z.; Chen, B.; Zhang, J.; Xia, G.; Hu, J.; Graff, G.; Liu, J.; Yang, Z., A Stable Vanadium Redox-Flow Battery with High Energy Density for Large-Scale Energy Storage. *Advanced Energy Materials* **2011**, 1 (3), 394-400.
17. Kucharyson, J. F.; Cheng, L.; Tung, S. O.; Curtiss, L. A.; Thompson, L., Predicting the Potentials, Solubilities and Stabilities of Metal-Acetylacetonates for Non-Aqueous Redox Flow Batteries Using Density Functional Theory Calculations. *Journal of Materials Chemistry A* **2017**, 5 13700-13709.